The Eurasia Proceedings of Science, Technology, Engineering & Mathematics (EPSTEM)
ISSN: 2602-3199

The Eurasia Proceedings of Science, Technology, Engineering & Mathematics (EPSTEM), 2023

Volume 26, Pages 604-623

IConTES 2023: International Conference on Technology, Engineering and Science

Numerical Modeling and Simulation of a Poroelastic Journal Bearing Lubricated By Nanofluids with Couple-Stresses

Mustapha Lahmar
University 8th may 1945 Guelma

Ammar Athmania
University 8th may 1945 Guelma

Benyebka Bou-Said
University of Lyon

Abstract: In this paper we present a numerical simulation of a porous journal bearing considering the fluid film – poroelastic matrix interaction and the non-Newtonian rheological behavior of nanolubricant consisting of base fluid and nanoparticles (NPs). The flow of nanolubricant in the bearing clearance space is described by the Vijay Kumar Stokes micro-continuum theory which considers the characteristic size of nanoparticles such as fullerenes dispersed in a base oil. The flow of the nanolubricant in the porous medium is modeled by the modified Darcy's law where the Beavers–Joseph slip conditions are applied at the fluid film-porous matrix interface. The deformation of the fluid-film porous matrix interface due to hydrodynamic pressure is calculated by using a simplified analytical thin elastic liner model. The hydrodynamic behavior of lubricating film is governed by the modified Reynolds equation obtained from the momentum, moment of momentum, and mass conservation laws using the classical Reynolds derivation process. The bearing porosity is introduced into the governing modified Reynolds equation by means of the Morgan-Cameron approximation. The steady-state analysis shows that for an imposed operating eccentricity, the load capacity increases with the characteristic size and the concentration of NPs while the attitude angle, the leakage flow rate, and the coefficient of friction decrease. On the other hand, the permeability decreases the hydrodynamic pressure, the load capacity, and the leakage flow rate, and increases the attitude angle and the coefficient of friction.

Keywords: Poro-elasto-hydrodynamic lubrication, Porous bearings, Nanoparticle, Non-Newtonian fluid.

Introduction

The plain journal bearings are widely used as machine elements in both rotating and reciprocating machinery. The porous journal bearing is a specific cost-efficient and eco-friendly type of plain journal bearing which comprises a pervious bush that is filled with lubricant giving it self-lubricating properties. Thus, no additional lubrication circuit is necessary to supply the bearing because the saturated porous matrix plays the role of lubricant reservoir.

As in any fluid bearing, the shaft axis is eccentric with respect to the bearing axis under the effect of the applied load, thereby creating a convergent-divergent film geometry. The rotation of the shaft causes an increase of pressure in the convergent region, and a decrease in the divergent part, up to a limit value of cavitation or saturation vapor pressure (Figure 1).

Increasingly, the use of porous bearings is extended to severe operating conditions such as higher applied loads often with changing direction, and higher rotor speeds. Instead of numerous steady-state analyses that are often

proposed in technical literature, accurate static and dynamical models are required to investigate the bearing's behavior under such operating conditions. They are widely used in different areas: computers, electric motors, automobiles (motor starters), and so on. Porous or self-lubricating bearings have been the subject of numerous research works since the early work from (Morgan & Cameron, 1957). Given the huge number of theoretical and experimental investigations carried out on both liquid and gas-lubricated porous bearings, we can cite the recent non exhaustive list of papers Morgan and Cameron (1957), Rouleau et al. (1974), Krieger and Dougherty (1959), Elsharkawy et al. (2001), Naduvinamani et al. (2002), Kaneko et al. (1994), Prakash et al. (1974).

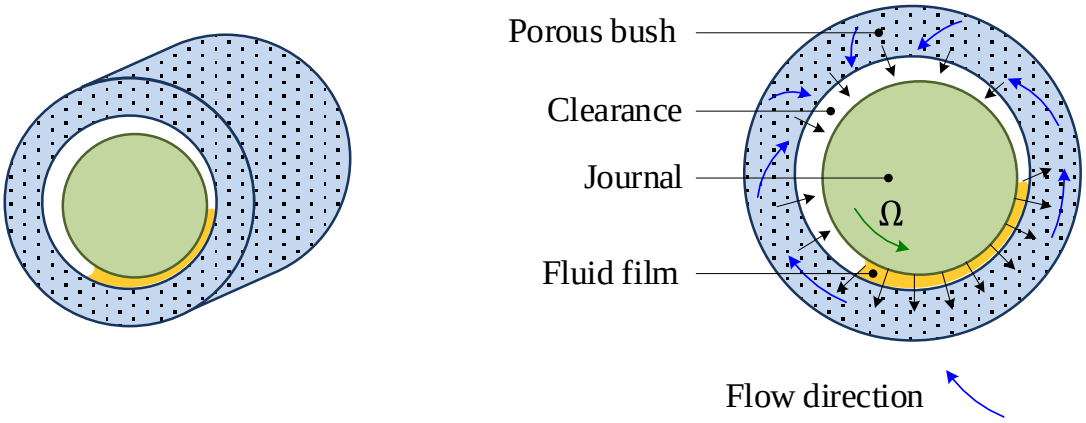

Figure 1 Schematic representation of a porous plain bearing with visualization of the streamlines of the lubricant flow.

Many theoretical studies have used the traditional Darcy's model (Darcy, 1856; Mokhtar et al., 1984) to describe the linear viscous (Newtonian) fluid flow in the porous bearing. The fluid model used does not consider the effects of the viscous forces of the lubricant infiltrating through the porous layer, which are at the origin of the generation of boundary layers. (Beavers and Joseph, 1967) experimentally showed that fluid slip can occur at the fluid film-porous layer interface (figure 2). They suggested replacing the boundary layer effect with appropriate slip conditions. According to the technical literature, several authors have applied such conditions to study non-deformable porous bearings lubricated by fluids with Newtonian rheological behavior (Lin, 1993,1994; Trachsel, 2017).

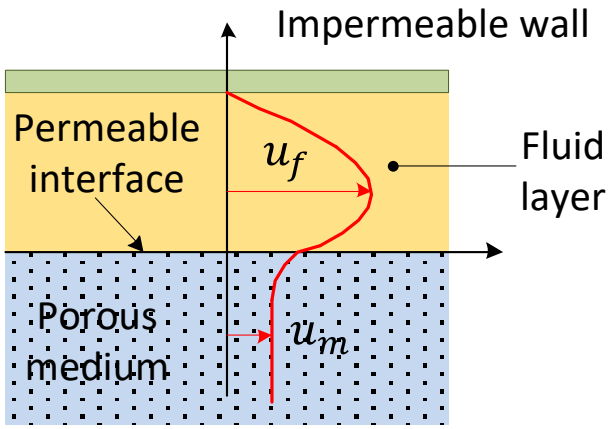

Figure 2. Typical velocity profiles of a unidirectional flow in the fluid film and the saturated porous medium.

Nowadays, with the progress of modern industry, the use of a non-Newtonian lubricant is becoming more and more interesting. Experimental studies Oliver (1988) and Scott et al. (1995) have shown that a base oil mixed with molecular additives or nanoparticles significantly improves the lubrication properties and thus reduces friction and wear, especially during the start-up and shutdown phases of machines.

Accordingly, the flow cannot be described by the classical continuum theory based on the classical Newtonian Navier-Stokes equations which neglects the size of the particles present in the doped oils. Several theoretical models to describe the flow of such complex fluids include the Vijay Kumar Stokes model Stokes (1965), Stokes (1984), Ariman et al. (1974) based on the micro-polar theory have been proposed in literature. The Vijay

Kumar Stokes fluid model, inspired from the theoretical work of Cosserat brothers (Cosserat E. & Cosserat F., (1909) for polar elastic media, considers polar effects in the form of couple stresses and body couples in addition to the surface and body forces. So, the flow of fluids with surface forces and couple-stresses is described by the theory of polar media which considers the effects of micrometric or nanometric size of the nano-additives or the agglomerates of nano-particles suspended in the base lubricant. In addition to the non-Newtonian rheological behavior of the fluid film, it is necessary to consider the deformation of the porous material, due to the high pressures generated in the film. Studies have already been carried out on rigid porous bearings lubricated by non-Newtonian couple stress fluid with a porous bearing containing a Newtonian fluid Bujurke et al. (1991), Naduvinamani (2001), and on deformable porous bearings lubricated by Newtonian fluid (Mak, 1977), Lin et al. (1996), (Elsharkawy, 2001).

The thrust of this paper is to investigate the combined effects of the characteristic size and concentration of nanoparticles or their aggregates such as inorganic fullerene (IF-WS2 NPs) or (IF-MoS2 NPs) on the steady-state performance characteristics of a porous journal bearing using nanofluids as lubricants. It is assumed that the journal (crankshaft) currently made of a forged steel is rigid and the bearing consists of a thin poro-elastic liner fixed in a stiff housing. The simplified thin elastic liner model (TELM), derived from an analytical elastic approach based on the use of complex Kolosov and Muskhelishvili potentials and Fourier series expansions (Lahmar, 1991, Lahmar, 2005).

The Reynolds' equation is derived in transient conditions and modified to account for the size of nanoparticles dispersed in the base lubricant, and the bearing-liner permeability property. This material property is introduced by means of the Morgan-Cameron approximation. In the proposed PEHD model, the normalized steady-state Reynolds equation is spatially discretized by the finite differences method using a nine point calculation molecule.

Bearing Description

Figure 3 shows the cross section of a porous plain bearing with the geometrical details. The plain bearing consists of two mechanical elements: the shaft and the bearing. The surfaces are assumed to be smooth. The shaft of radius R rotates around its axis with a peripheral or tangential constant speed $U=\Omega R$ with respect to the poroelastic matrix of thickness H, permeability k, Young's elasticity modulus E and Poisson's ratio υ. The shaft and the porous bearing are assumed to be aligned and separated by a non-Newtonian fluid film of thickness h.

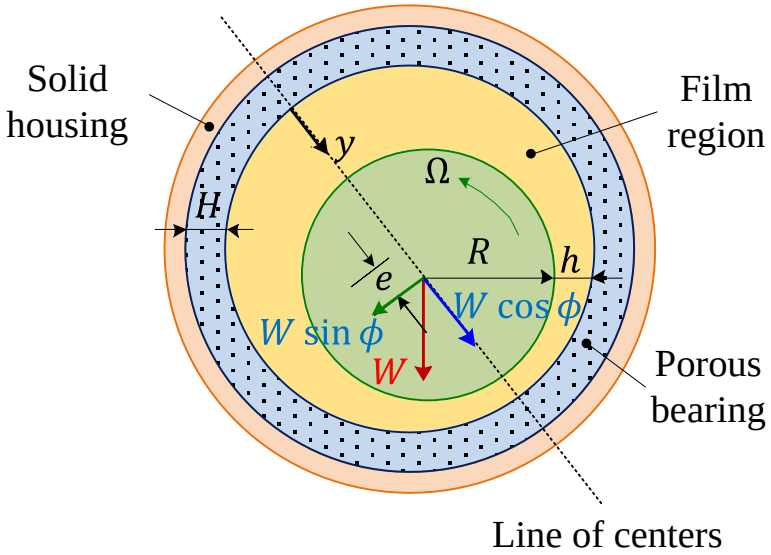

Figure 3. Geometric configuration of a porous journal bearing.

Basic Equations

The nanolubricant is modeled as a non-Newtonian couple stress fluid. In the absence of body couples and body forces, the V. K. Stokes couple stress fluid motion equation is written as follows:

$$\frac{1}{\nu}\left(\frac{\partial\vec{v}}{\partial t}+\vec{v}\,\overline{\overline{\mathrm{grad}\vec{v}}}\right)=-\frac{1}{\mu}\vec{\nabla}p+\vec{\nabla}^2\vec{v}-\ell^2\vec{\nabla}^4\vec{v} \tag{1}$$

where $\ell=\sqrt{\eta/\mu}$ is a characteristic size of nanoparticles or agglomerates of NPs.

The dimensional analysis of the above equation (1) in the context of the viscous thin films theory significantly simplifies this equation which becomes:

$$\frac{\partial p}{\partial x}=\mu\frac{\partial^2 u}{\partial y^2}-\eta\frac{\partial^4 u}{\partial y^4} \tag{2}$$

$$\frac{\partial p}{\partial y}=0\rightarrow p=p(x,z) \tag{3}$$

$$\frac{\partial p}{\partial z}=\mu\frac{\partial^2 w}{\partial y^2}-\eta\frac{\partial^4 w}{\partial y^4} \tag{4}$$

We use the following kinematic boundary conditions:

• On the surface of the shaft $y=h$

$$u(x,h,z)=U(x,z)=\Omega R \tag{5-a}$$

$$v(x,h,z)=\frac{dh}{dt}=\frac{\partial h}{\partial t}+U\frac{\partial h}{\partial x}+W\frac{\partial h}{\partial z} \tag{5-b}$$

$$w(x,h,z)=W=0 \tag{5-c}$$

$$\left.\frac{\partial^2 u}{\partial y^2}\right|_{x,y=h,z}=0 \tag{5-d}$$

$$\left.\frac{\partial^2 w}{\partial y^2}\right|_{x,y=h,z}=0 \tag{5-e}$$

The conditions (5-d) and (5-e) express the nullity of the couple stresses on the surface of the shaft; i. e.

$$-2\eta\left.\frac{\partial^2 u}{\partial y^2}\right|_{x,y=h,z}=-2\eta\left.\frac{\partial^2 w}{\partial y^2}\right|_{x,y=h,z}=0$$

• At the bush fluid film-porous interface $y=0$

$$u(x,0,z)=U_b(x,z) \tag{6-a}$$

$$\left.\frac{\partial u}{\partial y}\right|_{x,y=0,z}=\frac{\alpha_b}{\sqrt{k}}(U_b-u^*) \tag{6-b}$$

$$v(x,0,z)=v^*(x,z) \tag{6-c}$$

$$w(x,0,z) = W_b(x,z) \tag{6-d}$$

$$\left.\frac{\partial w}{\partial y}\right|_{x,y=0,z} = \frac{\alpha_b}{\sqrt{k}}(W_b - w^*) \tag{6-e}$$

$$\left.\frac{\partial^2 u}{\partial y^2}\right|_{x,y=0,z} = 0 \tag{6-f}$$

$$\left.\frac{\partial^2 w}{\partial y^2}\right|_{x,y=0,z} = 0 \tag{6-g}$$

where U_b and W_b are respectively the Beavers-Joseph sliding velocities at the fluid film-porous interface along the x and z directions.

α_b is the dimensionless Beavers slip coefficient and k being the permeability of the isotropic porous layer's material in (m^2).

The conditions (6-f) and (6-g) reflect the nullity of the couple stresses at the interface due to the absence of rotation of the particles at the solid wall level, i.e.

$$-2\eta \left.\frac{\partial^2 u}{\partial y^2}\right|_{x,y=0,z} = -2\eta \left.\frac{\partial^2 w}{\partial y^2}\right|_{x,y=0,z} = 0$$

Equations (6-a), (6-b), (6-d), and (6-e) represent the Beavers-Joseph slip conditions and equation (6-c) explain the condition of continuity of the velocity along the normal to the fluid film-porous layer interface. u^*, v^*, w^* are respectively the components of the velocity vector of the fluid with particles along the x, y, and z directions at the interface. These velocities are calculated by the following modified Darcy's law:

$$u^* = -\frac{k}{\mu(1-\beta)}\frac{\partial p^*}{\partial x} \tag{7-a}$$

$$v^* = -\frac{k}{\mu(1-\beta)}\frac{\partial p^*}{\partial y} \tag{7-b}$$

$$w^* = -\frac{k}{\mu(1-\beta)}\frac{\partial p^*}{\partial z} \tag{7-c}$$

or in more condensed form: $\vec{v}^* = -\frac{k}{\mu(1-\beta)}\vec{\nabla}p^*$

where $\beta = \ell^2/k$ is the percolation (or penetration) parameter of the particles in the porous matrix and p^* is the pressure in the porous medium obtained from the solution of Laplace's equation (8) :

$$\vec{\nabla}^2 p^*(x,y,z) = \frac{\partial^2 p^*}{\partial x^2} + \frac{\partial^2 p^*}{\partial y^2} + \frac{\partial^2 p^*}{\partial z^2} = 0 \tag{8}$$

with: $0 \le x \le 2\pi R$; $-H \le y \le 0$; $-\frac{L}{2} \le z \le \frac{L}{2}$.

The boundary conditions associated to the Laplace equation (8) are:

In the middle section of the bearing assumed to be aligned ($z = 0$), the pressure is maximum (axial symmetry of the pressure profile) :

$$\left.\frac{\partial p^*}{\partial z}\right|_{x,y,z=0} = 0 \tag{9-a}$$

On the edges (ends) of the porous bearing ($z = \pm L/2$), the absolute pressure of the fluid in the porous matrix is taken equal to the atmospheric pressure:

$$p^*|_{x,y,z=L/2} = 0 \tag{9-b}$$

In the case where the edges of the bearing are sealed, condition (9-b) will be replaced by the following condition:

$$\left.\frac{\partial p^*}{\partial z}\right|_{x,y,z=\pm L/2} = 0 \tag{9-c}$$

Pressure periodicity condition:

$$p^*(\theta, y, z) = p^*(\theta + 2\pi, y, z) \tag{9-d}$$

$\theta = x/R$ being the circumferential coordinate of the bearing ($0 \leq \theta \leq 2\pi$).

On the outer surface of the porous coating, $y = -H$, the impermeability condition is written:

$$\left.\frac{\partial p^*}{\partial y}\right|_{x,y=-H,z} = 0$$

At the fluid film-porous layer interface, $y = 0$, the pressure continuity condition is applied:

$$p^*|_{x,y=0,z} = p|_{x,z} \tag{9-e}$$

Given the appropriate boundary conditions (5), (6) one can obtain:

$$u(x,y,z) = \frac{U}{h}y + U_b(x,z)\left(1 - \frac{y}{h}\right) + \frac{1}{2\mu}\frac{\partial p}{\partial x}\left\{y(y-h) + 2\ell^2\left[1 - \frac{\cosh\left(\frac{h-2y}{2\ell}\right)}{\cosh\left(\frac{h}{2\ell}\right)}\right]\right\} \tag{10}$$

$$w(x,y,z) = W_b(x,z)\left(1 - \frac{y}{h}\right) + \frac{1}{2\mu}\frac{\partial p}{\partial z}\left\{y(y-h) + 2\ell^2\left[1 - \frac{\cosh\left(\frac{h-2y}{2\ell}\right)}{\cosh\left(\frac{h}{2\ell}\right)}\right]\right\} \tag{11}$$

The Beavers-Joseph slip velocities U_b and W_b are obtained by inserting the analytical expressions of u and w (Eq. 10) and (Eq. 11) respectively in the equations (6-b) and (6-e) :

$$U_b(x,z) = \frac{1}{\alpha_b\sigma + 1}\left\{U + \alpha_b\sigma\, u^*(x,0,z) + \frac{1}{2\mu}\frac{\partial p}{\partial x}\left[-h^2 + 2h\ell\tanh\left(\frac{h}{2\ell}\right)\right]\right\} \tag{12-a}$$

$$W_b(x,z) = \frac{1}{\alpha_b\sigma + 1}\left\{\alpha_b\sigma\, w^*(x,0,z) + \frac{1}{2\mu}\frac{\partial p}{\partial z}\left[-h^2 + 2h\ell\tanh\left(\frac{h}{2\ell}\right)\right]\right\} \tag{12-b}$$

with $\sigma = \frac{h}{\sqrt{k}}$, $u^*(x,0,z) = -\frac{k}{\mu(1-\beta)}\frac{\partial p}{\partial x}$, $w^*(x,0,z) = -\frac{k}{\mu(1-\beta)}\frac{\partial p}{\partial z}$.

The velocities u and w of the flow can also be expressed in the following form:

$$u(x,y,z) = \frac{U}{h}[y(1-\xi_0) + h\xi_0] + \frac{1}{2\mu}\frac{\partial p}{\partial x}\left\{(y-h)\left[y + \frac{h}{3}\xi_1 - 2\ell\xi_0\tanh\left(\frac{h}{2\ell}\right)\right] + 2\ell^2\left[1 - \frac{\cosh\left(\frac{2y-h}{2\ell}\right)}{\cosh\left(\frac{h}{2\ell}\right)}\right]\right\} \tag{13}$$

and

$$w(x,y,z) = \frac{1}{2\mu}\frac{\partial p}{\partial z}\left\{(y-h)\left[y + \frac{h}{3}\xi_1 - 2\ell\xi_0\tanh\left(\frac{h}{2\ell}\right)\right] + 2\ell^2\left[1 - \frac{\cosh\left(\frac{2y-h}{2\ell}\right)}{\cosh\left(\frac{h}{2\ell}\right)}\right]\right\} \tag{14}$$

With $\xi_0 = \frac{1}{\alpha_b\sigma+1} = \frac{\sqrt{k}/\alpha_b}{h+\sqrt{k}/\alpha_b}$ and $\xi_1 = \frac{3\left(\frac{2k}{1-\beta}+h\frac{\sqrt{k}}{\alpha_b}\right)}{h\left(\frac{\sqrt{k}}{\alpha_b}+h\right)}$

Substituting the analytical expressions of $u(x,y,z)$ and $w(x,y,z)$ in the continuity equation then integrating across the film thickness gives:

$$\frac{\partial}{\partial x}\left[f(h,\ell,k)\frac{\partial p}{\partial x}\right] + \frac{\partial}{\partial z}\left[f(h,\ell,k)\frac{\partial p}{\partial z}\right] = 6\mu U\frac{\partial}{\partial x}[h(1+\xi_0)] + 12\frac{k}{1-\beta}\frac{\partial p^*}{\partial y}\bigg|_{x,y=0,z} + 12\mu\frac{\partial h}{\partial t} \tag{15}$$

with $f(h,\ell,k) = h^3(1+\xi_1) - 6h^2\ell\,\xi_0\tanh\left(\frac{h}{2\ell}\right) - 12\ell^2\left[h - 2\ell\tanh\left(\frac{h}{2\ell}\right)\right]$

From the Morgan-Cameron approximation for a very thin, porous layer $(H/R \ll 1)$ we can express $\partial p^*/\partial y$ at the fluid film-porous layer interface $(y=0)$ as follows:

$$\frac{\partial p^*}{\partial y}\bigg|_{x,y=0,z} = -H\left(\frac{\partial^2 p}{\partial x^2} + \frac{\partial^2 p}{\partial z^2}\right) \tag{16}$$

Finally, we obtain the following modified Reynolds equation :

$$\begin{aligned}\frac{\partial}{\partial x}\left\{\left[h^3(1+\xi_1) - 6h^2\ell\,\xi_0\tanh\left(\frac{h}{2\ell}\right) - 12\,\ell^2\left(h - 2\ell\tanh\left(\frac{h}{2\ell}\right)\right) + \frac{12kH}{(1-\beta)}\right]\frac{\partial p}{\partial x}\right\} \\ + \frac{\partial}{\partial z}\left\{\left[h^3(1+\xi_1) - 6h^2\ell\,\xi_0\tanh\left(\frac{h}{2\ell}\right) - 12\ell^2\left(h - 2\ell\tanh\left(\frac{h}{2\ell}\right)\right) + \frac{12kH}{(1-\beta)}\right]\frac{\partial p}{\partial z}\right\} \\ = 6\mu U\frac{\partial}{\partial x}[h(1+\xi_0)] + 12\mu\frac{\partial h}{\partial t}\end{aligned} \tag{17}$$

The modified Reynolds equation (17) is a nonlinear partial differential equation whose the main unknown is the hydrodynamic pressure p. This equation is coupled to the film geometric equation:

$$h(\theta,z,t) = C(1+\varepsilon\cos\theta) + \mathcal{L}\,p \tag{18}$$

where $C = R_b - R$ is the bearing radial clearance, $\varepsilon = e/C$ is the relative operating eccentricity, $\theta = \frac{x}{R}$ is the bearing angle, and $\mathcal{L} = \frac{(1+\upsilon)(1-2\upsilon)}{1-\upsilon}\frac{H}{E}$ is the compliance operator. The parameters appearing in the expression of $\mathcal{L}$ are the Young's elasticity modulus E, the Poisson's ratio υ, and the thickness of the poroelastic layer H.

Boundary Conditions

The pressure field in the lubricating film must satisfy the modified Reynolds equation (17) and the following boundary conditions:

In the middle section of the aligned bearing $(z = 0)$, the pressure being maximum, i.e.: $\left.\frac{\partial p}{\partial z}\right|_{x,z=0,t} = 0$

On the two free edges of the bearing $(z = \pm L/2)$, the absolute pressure in the fluid film is assumed to be equal to atmospheric pressure, i. e. : $p(x, z = \pm L/2, t) = 0$

The pressure field is assumed to be periodic in the circumferential direction, i.e.: $p(2\pi R, z, t) = p(0, z, t)$
In addition to the aforementioned conditions, the Swift-Stieber conditions related to the flow of the fluid in the bearing are considered:

$$p(x_c,z,t) = \left.\frac{\partial p}{\partial x}\right|_{x_c,z,t} = \left.\frac{\partial p}{\partial z}\right|_{x_c,z,t} = 0$$

where x_c is the break abscissa of the film (cavitation) which is an additional unknown of the problem.

Equation (17) can be rewritten in dimensionless form for the numerical treatment. For this, we use for the spatial coordinates : $\theta = x/R$, $\bar{z} = z/L$; for the velocity components : $\bar{u} = u/U$, $\bar{v} = Lv/(UC)$, $\bar{w} = w/U$; for the the fluid film pressure: $\bar{p} = C^2p/(\mu_0 UR)$; for the film thickness : $\bar{h} = h/C$; for the fluid dynamic viscosity : $\bar{\mu} = \mu/\mu_0$ with μ_0 the reference viscosity, and finally for the characteristic size of the nanoparticles $\bar{\ell} = \ell/C$.

This change of variables leads to the normalized stationary modified Reynolds equation (19):

$$\frac{\partial}{\partial\theta}\left[\bar{G}(\bar{h},\bar{\ell},K)\frac{\partial\bar{p}}{\partial\theta}\right] + \left(\frac{R}{L}\right)^2\frac{\partial}{\partial\bar{z}}\left[\bar{G}(\bar{h},\bar{l},K)\frac{\partial\bar{p}}{\partial\bar{z}}\right] = 6\bar{\mu}\frac{\partial}{\partial\theta}[\bar{h}(1+\xi_0)] \tag{19}$$

where $\bar{\mu} = \left(1-\frac{\phi}{\phi_m}\right)^{-[\eta]\phi_m}$ is the relative viscosity of the nanolubricant considered as a suspension according to the Krieger-Dougherty model, and

$$\bar{G}(\bar{h},\bar{\ell},K) = \bar{h}^3(1+\xi_1) - 12\bar{\ell}^2\left[\bar{h} - 2\bar{\ell}\tanh\left(\frac{\bar{h}}{2\bar{\ell}}\right)\right] - 6\bar{h}^2\bar{\ell}\,\xi_0\tanh\left(\frac{\bar{h}}{2\bar{\ell}}\right) + \frac{12\,K\bar{H}}{(1-\beta)}$$

$K = kR/C^3$ and $\bar{H} = H/R$ are the dimensionless permeability and the relative thickness of the porous coating, respectively. Equation (18) can be written in its normalized form as

$$\bar{h}(\theta,z,t) = 1 + \varepsilon\cos\theta + \bar{\mathcal{L}}\,\bar{p} \quad \text{where} \quad \bar{\mathcal{L}} = \frac{(1-2\upsilon)(1+\upsilon)}{1-\upsilon}\frac{\mu_0\omega_J\left(\frac{R}{C}\right)^3}{E}\bar{H} \tag{20}$$

Figure 4 shows a typical variation of the relative viscosity $\bar{\mu} = \mu/\mu_0$ as a function of the volume fraction ϕ calculated by the Krieger-Dougherty viscosity model.

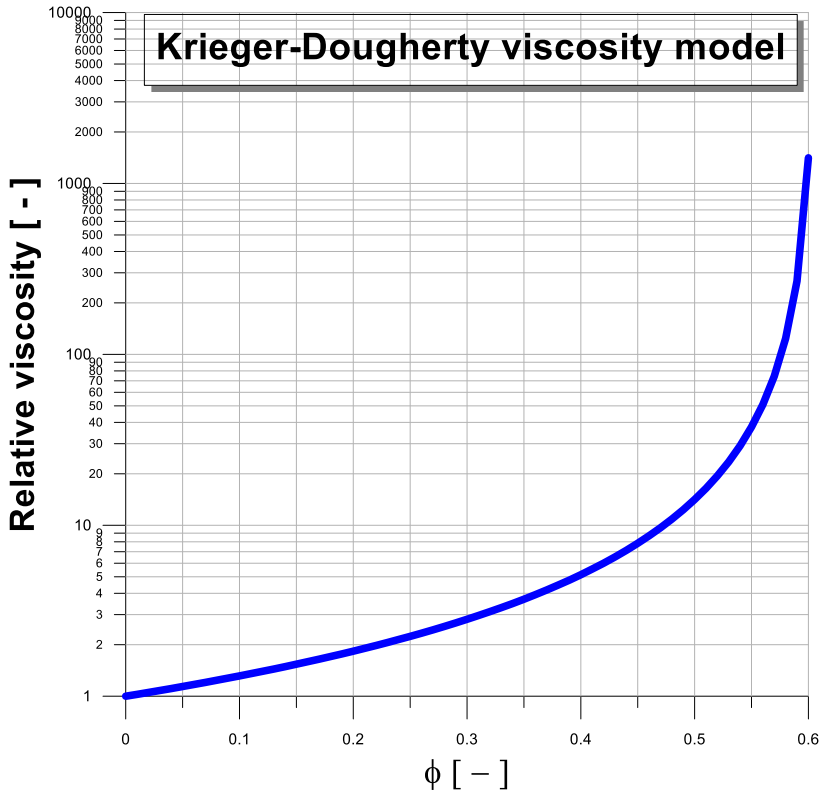

Figure 4. Graphical representation of the Krieger-Dougherty viscosity model for a range of volume fraction and $\phi_m = 0.605$

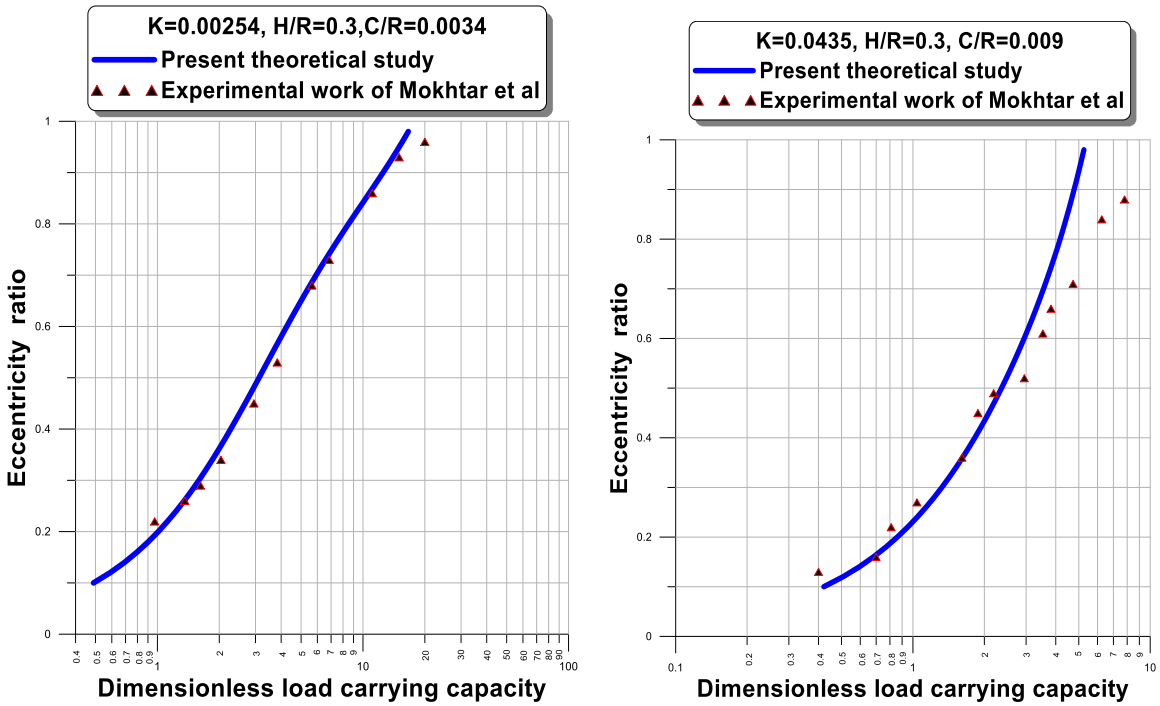

Figure 5. Comparison of dimensionless load capacity with experimental data for two values of K and $\frac{C}{R}$.

Validation

The coupled equations (19) and (20) with the associated boundary conditions are solved numerically using finite differences method and a numerical iterative scheme with under-relaxation coefficient. To validate the model, we compare the obtained results with the experimental data of Mokhtar et al. For this, the following data were considered:

$R = 9.5 \times 10^{-3}\ m$, $L = 0.033\ m$, $C = 32$ and $85.5\ \mu m$, $H = 3.0225 \times 10^{-3}\ m$, $k = 8.76 \times 10^{-15}$ and $2.86 \times 10^{-12}\ m^2$.

Figure 5 depicts the evolution of the dimensionless carrying capacity against eccentricity ratio $\varepsilon = \frac{e}{C}$.

This figure shows that the numerical predictions are in perfect agreement with the experimental data. However, a deviation can be observed for large relative eccentricities especially in the case of high permeability. This discrepancy can be attributed to thermal effects which are neglected in the present study. To further validate the model, we compare, in Table 1, our obtained results with those published by Rouleau et al. for different values of the operating eccentricity ratios and the dimensionless permeability of the porous layer.

Calculations are performed for the case of a finite length bearing with a longitudinal feeding groove using the Morgan-Cameron approximation as well as cavitation Reynolds boundary conditions. On the other hand, the slip phenomenon occurring at the interface is not considered in these calculations. According to the results presented in this table, we can conclude that the Morgan-Cameron approximation used in the proposed numerical model gives good results especially for a thin porous layer and this for the different simulated cases. We recall:

$\bar{F} = \frac{W}{\frac{\mu_0 U R^2 L}{C^2}} = \sqrt{\bar{F}_X^2 + \bar{F}_Y^2}$ where $\bar{F}_X, \bar{F}_Y$ are the load components along the direction of the applied load (X −axis) and the normal to the latter (Y −axis)

$\bar{F}_X = 2\int_{\bar{z}=0}^{\bar{z}=1/2}\int_{\theta=0}^{\theta=\theta_c} \bar{p}\cos\theta d\theta\, d\bar{z}$ and $\bar{F}_Y = 2\int_{\bar{z}=0}^{\bar{z}=1/2}\int_{\theta=0}^{\theta=\theta_c} \bar{p}\sin\theta d\theta\, d\bar{z}$ .The attitude angle is given by :

$\varphi = \tan^{-1}\left(\frac{\bar{F}_Y}{\bar{F}_X}\right)$. The friction force is: $\bar{F}_f = \frac{F_f}{\frac{\mu_0 U R L}{C}}$ with $F_f = \|\vec{F_f}\| = \sqrt{{F_f}_1^2 + {F_f}_2^2}$

${F_f}_1 = 2\int_0^{L/2}\int_0^{2\pi} \tau_{xy}\big|_{x,y=h,z} R d\theta dz$ and ${F_f}_2 = 2\int_0^{L/2}\int_0^{2\pi} \tau_{zy}\big|_{x,y=h,z} R d\theta dz$ are the friction force components of $\vec{F_f}$ in θ and z-axis direction, respectively. In these relationships, the wall shear stresses express as

$\tau_{xy}\big|_{y=h} = \mu\frac{\partial u}{\partial y}\Big|_{y=h} = \mu\frac{U}{h}(1-\xi_0) + \frac{h}{2}\frac{\partial p}{\partial x}\left(1+\frac{\xi_1}{3}\right)$ and $\tau_{zy}\big|_{y=h} = \mu\frac{\partial w}{\partial y}\Big|_{y=h} = \frac{h}{2}\frac{\partial p}{\partial z}\left(1+\frac{\xi_1}{3}\right)$

The friction coefficient and friction number are given by the following relationships:

$C_f = \frac{C}{R}\frac{\bar{F}_f}{\bar{F}}$ and $f = \frac{R}{C}C_f = \frac{\bar{F}_f}{\bar{F}}$

Table 1. Comparison of the theoretical results obtained by the developed computer code with those published by Rouleau et al. for : $R/L = 0.5$; $H/R = 0.2$; $C/R = 0.001$

ε	K	$\overline{F}$	$f\left(\frac{R}{C}\right)$	$\Phi\ (degrees)$	Note
0.80	0.001	**6.9215**	**1.7465**	**35.7342**	**Rouleau et al.**
		6.7472	**1.7337**	**37.1612**	**Present study**
		0.0251	**0.0073**	**0.0399**	**Relative discrepancy (%)**
	1.000	**0.5296**	**20.1582**	**73.4712**	**Rouleau et al.**
		0.5536	**19.3003**	**73.1705**	**Present study**
		0.0453	**0.0426**	**0.0041**	**Relative discrepancy (%)**
	10.000	**0.0658**	**---**	**84.4858**	**1**
		0.0794	**132.3135**	**82.8903**	**Present study**
		0.2066	**---**	**0.0188**	**Relative discrepancy (%)**
0.60	0.001	**2.6126**	**3.2355**	**49.8640**	**Rouleau et al.**
		2.6041	**3.2482**	**50.7268**	**Present study**
		0.0032	**0.0039**	**0.0173**	**Relative discrepancy (%)**
	1.000	**0.4080**	**19.5417**	**75.8843**	**Rouleau et al.**
		0.4271	**18.6807**	**75.5757**	**Present study**
		0.0468	**0.0441**	**0.0041**	**Relative discrepancy (%)**
	10.000	**0.0499**	**---**	**84.9922**	**Rouleau et al.**
		0.0602	**130.7896**	**83.4594**	**Present study**
		0.2064	**---**	**0.0180**	**Relative discrepancy (%)**
0.20	0.001	**0.4984**	**12.9634**	**73.5610**	**Rouleau et al.**
		0.5025	**12.8589**	**73.8830**	**Present study**
		0.0082	**0.0080**	**0.0043**	**Relative discrepancy (%)**
	1.000	**0.1395**	**46.0617**	**81.8352**	**1**
		0.1464	**43.9127**	**81.5428**	**2**
		0.0501	**0.0467**	**0.0035**	**Relative discrepancy (%)**
	10.000	**0.0168**	**---**	**85.8865**	**1**
		0.0203	**315.8283**	**84.4840**	**2**
		0.2083	**---**	**0.0118**	**Relative discrepancy (%)**

Parametric Study

In the following, the relevant calculation results are obtained using the geometric data and the operating conditions reported in Table 2 below. We analyze the effects of key design parameters on the steady-state performance characteristics of a finite length porous journal bearing, namely: the hydrodynamic pressure profile in the middle section of the bearing $\bar{p}$, the load capacity $\bar{F}$, the leakage flow rate $\bar{Q}$, the coefficient of friction $f\left(\frac{R}{C}\right)$, and the attitude angle φ. These key parameters are: the size of NPs (or agglomerates of NPs) characterized by the normalized couple stress parameter $\bar{\ell} = \ell/C$, the non-dimensional parameters of permeability and elasticity $K = kR/C^3$ and $\bar{\mathcal{L}}$ of the poroelastic matrix, the concentration of NPs in the base fluid ϕ, and the Joseph-Beavers slip coefficient α_b .

Effects of the Characteristic Size of NPs or Agglomerates of NPs

Figure 6 represents the circumferential variation of the dimensionless pressure $\bar{p}$ calculated in the middle section of the bearing, $\bar{z} = 0$, for different values of the characteristic diameter $\bar{\ell}$ of the NPs (fullerenes IF WS2 or IF MoS2) dispersed in the base lubricant, $\varepsilon = 0.8$, $K = 2.54 \times 10^{-3}$, $\phi = 0.$, and $\bar{\mathcal{L}} = 1.15 \times 10^{-4}$. It is observed that the use of a nano-lubricant (base fluid + nano-additives) whose behavior is naturally non-Newtonian leads to a greater increase in the pressure peak compared to the case of the lubricant without additives. Nano-additives or agglomerates of NPs, mixed with the lubricant, oppose the movement of the fluid and thus further improve the pressure in the fluid film.

Table 2. Bearing geometric characteristics and operating conditions.

Bearing length, (m)	L	33×10^{-3}
Shaft radius, (*m*)	R	9.5×10^{-3}
Radial clearance, (*m*)	C	85.5×10^{-6}
Shaft rotation velocity, (*rpm*)	Ω	870.
Porous thickness coating, (*m*)	H	3×10^{-3}
Porous coating permeability, (m^2)	k	0., 2.86×10^{-12}
Sliding parameter (dimensionless)	α_b	0.1
Penetration (percolation) coefficient	β	0.0
Young's modulus, (*GPa*) Bronze porous (Hamrock, 2004)	E	60.
Poisson's ratio (-) Bronze porous (Hamrock, 2004)	υ	0.22
Kinematic viscosity of the base oil $(SAE\ 30)\ at$ 40 °C, (*cSt* or mm^2/s)	ν_0	106.6
Lubricant density $(SAE\ 30)\ at$ 20 °C, (kg/m^3)	ρ_0	888.
Relative characteristic diameter of NPs (-)	ℓ/C	0., 0.1, 0.4
Volume fraction of NPs, (-)	ϕ	0., 25 %

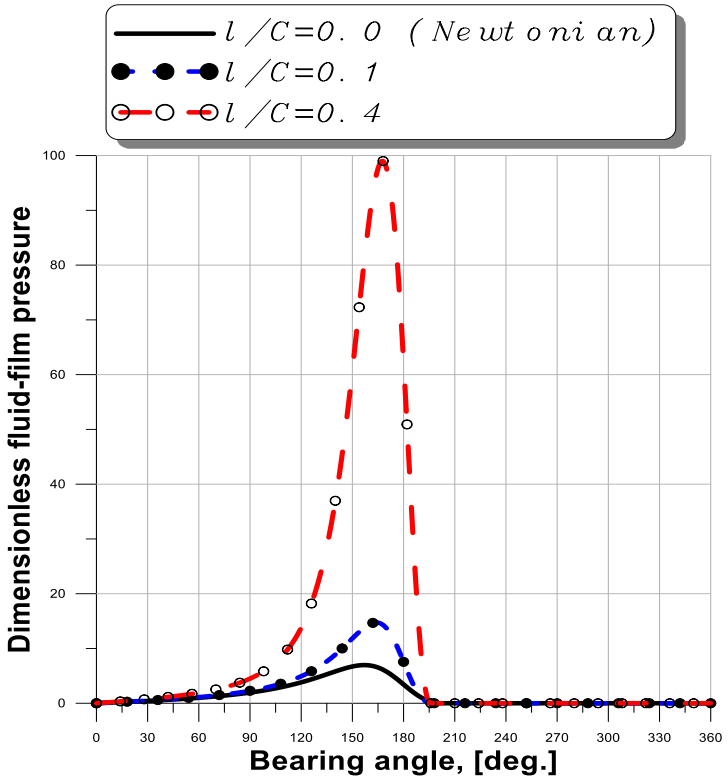

Figure 6. Calculated pressure profiles in the mid-section $(\bar{z} = 0)$ for different values of the characteristic diameter of NPs, $\varepsilon = 0.8$; $K = 2.54 \times 10^{-3}$; $= 0.$; $\bar{\mathcal{L}} = 1.15 \times 10^{-4}$ *and* $\alpha_b = 0.$

Figure 7 depicts the evolution of the dimensionless load capacity $\bar{F}$ as a function of the eccentricity ratio for different values of the characteristic diameter of the NPs $\bar{\ell}$ *for* $K = 2.54 \times 10^{-3}$, $\phi = 0.$, *and* $\bar{\mathcal{L}} = 1.15 \times 10^{-4}$. As in the case of the hydrodynamic pressure, the size of the NPs increases significantly the hydrodynamic lift, $\bar{F}$, of the journal bearing system. This is due to the flow resistance generated by the additives mixed into the lubricant. As expected, a large increase in $\bar{F}$ is observed for high values of the operating eccentricity ratio ε.

Figure 8 shows the variation of the bearing attitude angle, φ, versus the operating eccentricity ratio ε for different values of the characteristic diameter of the NPs $\bar{\ell}$, $K = 2.54 \times 10^{-3}$, $\phi = 0.$, *and* $\bar{\mathcal{L}} = 1.15 \times 10^{-4}$.

For a same value of eccentricity ratio, the increase in $\bar{\ell}$ leads to a significant decrease in the attitude angle, especially when the nano-lubricant contains large NPs or agglomerates of NPs. It can be concluded that the presence of large NPs plays a positive role with respect to the dynamic stability of the bearing. This can be confirmed through a more complete linear dynamic study based on the calculation of the stiffness and damping coefficients of the bearing.

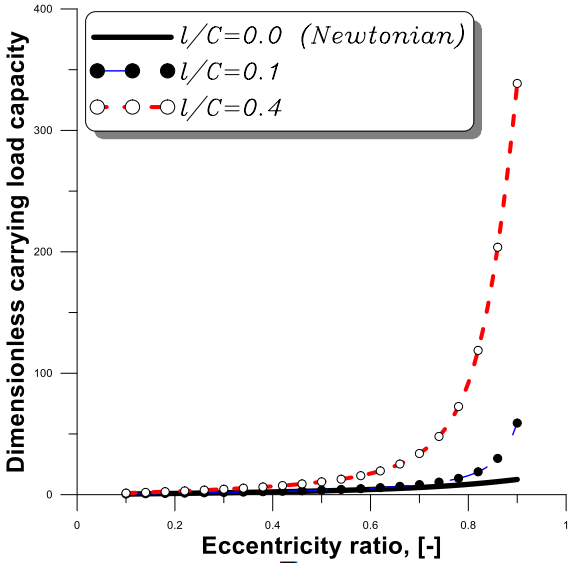

Figure 7. Evolution of the dimensionless load capacity $\bar{F}$ as a function of the eccentricity for different values of the characteristic size of the NPs, $K = 2.54 \times 10^{-3}$; $\phi = 0.$; $\bar{\mathcal{L}} = 1.15 \times 10^{-4}$ *and* $\alpha_b = 0.$

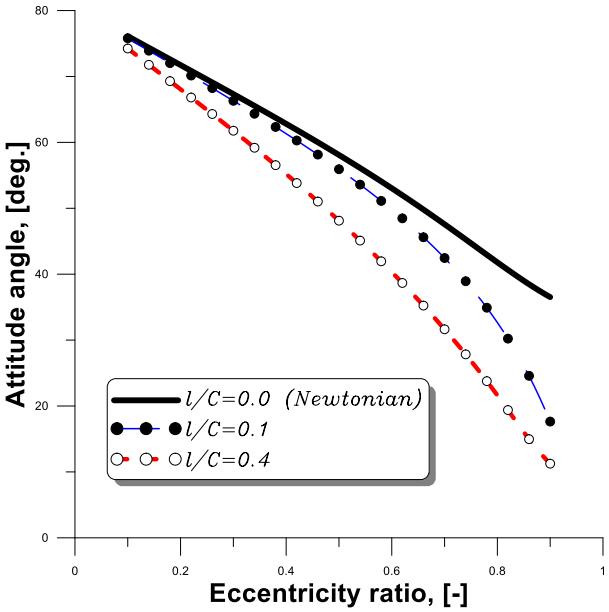

Figure 8. Variation of the attitude angle as a function of the eccentricity for different values of the characteristic size of the NPs, $\mathbf{K = 2.54 \times 10^{-3}}$; $\phi = 0.$; $\bar{\mathcal{L}} = 1.15 \times 10^{-4}$ *and* $\alpha_b = 0.$

Figure 9 gives the variation of the coefficient of friction, as a function of the eccentricity for different values of the characteristic diameter of the NPs $\bar{\ell}$ *for* $K = 2.54 \times 10^{-3}$, $\phi = 0.$,*and* $\bar{\mathcal{L}} = 1.15 \times 10^{-4}$. It is shown that the coefficient of friction decreases with the operating eccentricity. For a given value of eccentricity, the coefficient of friction calculated in the case of large NPs is clearly lower than that obtained in the case of NPs of small relative size. It should be noted that the frictional force acting on the surface of the shaft is calculated in excess assuming that the entire bearing surface is drained with lubricant.

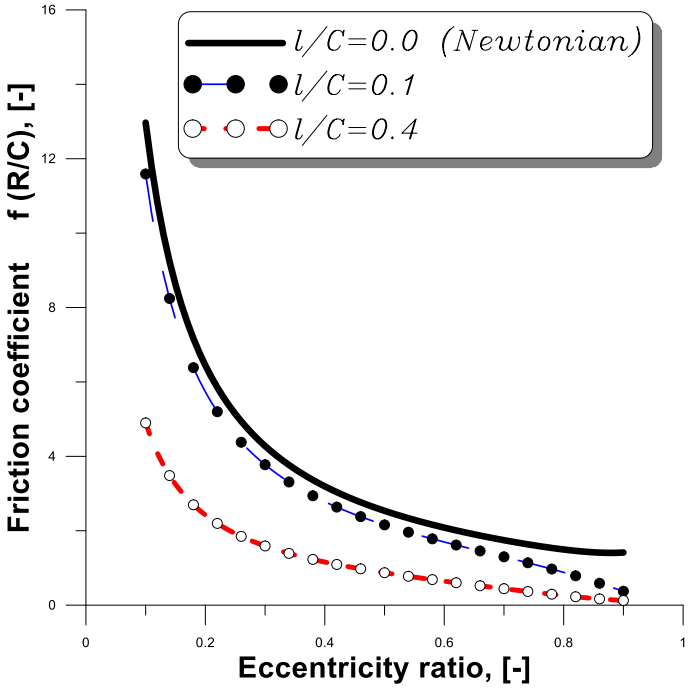

Figure 9. Evolution of the coefficient of friction $\boldsymbol{f(R/C)}$ for different values of the characteristic size of NPs, $\boldsymbol{K = 2.54 \times 10^{-3}}$; $\boldsymbol{\phi = 0.}$; $\boldsymbol{\bar{\mathcal{L}} = 1.15 \times 10^{-4}}$; $\boldsymbol{\alpha_b = 0.}$

Figure 10 shows the variation of the calculated dimensionless leakage flow at the free edges of the bearing, $\bar{Q}$, as a function of the eccentricity ratio ε for different values of the characteristic diameter of the NPs $\bar{\ell}$ *for* $K = 2.54 \times 10^{-3}$, $\phi = 0.$, *and* $\bar{\mathcal{L}} = 1.15 \times 10^{-4}$. The flow is calculated by integrating the average velocities $\bar{w}(x,z) = \frac{1}{h}\int_0^h w(x,y,z)dy$ of the flow at the two ends of the bearing $z = \pm L/2$. This figure clearly shows that the more the size of the NPs, $\bar{\ell}$, increases, the more the leakage rate decreases, especially for high operating eccentricities, i.e. when the bearing is moderately or heavily loaded.

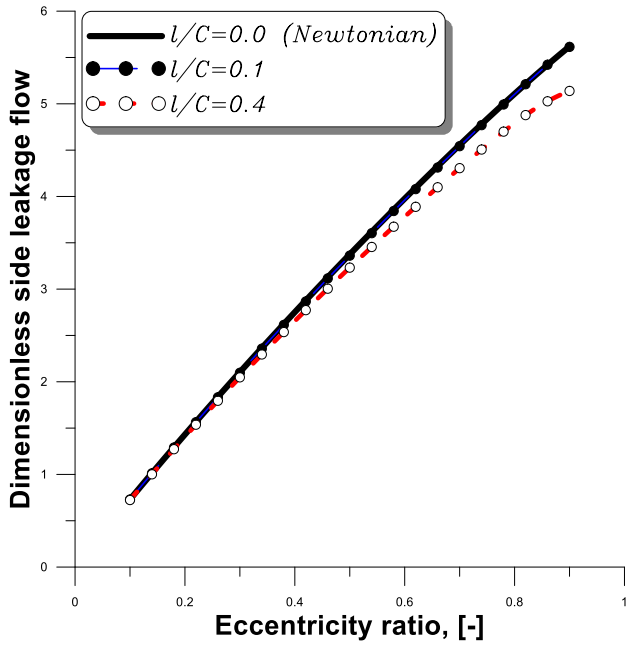

Figure 10. Variation of the leakage flow rate for different values of the characteristic size of the NPs, $\boldsymbol{K = 2.54 \times 10^{-3}}$; $\boldsymbol{\phi = 0}$; $\boldsymbol{\bar{\mathcal{L}} = 1.15 \times 10^{-4}}$; *and* $\boldsymbol{\alpha_b = 0.}$

Effects of Porous Layer Permeability

The calculated circumferential pressure distribution for different dimensionless permeability parameters K of the porous matrix, $\varepsilon = 0.6$, $\bar{\ell} = 0.1$, $\phi = 0.$, and $\bar{\mathcal{L}} = 1.15 \times 10^{-4}$ is shown in Figure 11. The pressure in the fluid film decreases significantly with the permeability parameter. This is explained by the fact that for large values of K i.e. for a larger number of pores, part of the lubricating fluid infiltrates more easily inside the porous matrix through the fluid-bearing film interface. Thus, the amount of fluid in the space between the shaft and bearing surfaces decreases which causes the pressure drop and hence the load capacity of the bearing $\bar{F}$ which corresponds to the area delimited by the pressure curve.

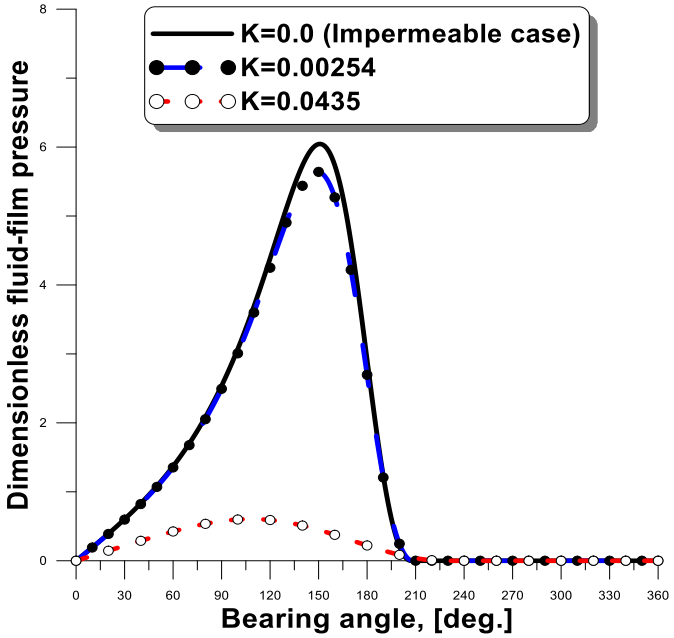

Figure 11. Pressure profile calculated at $\bar{z} = 0$ for different permeability parameters K, $\varepsilon = 0.6$; $\bar{\ell} = 0.1$; $\phi = 0.$; $\bar{\mathcal{L}} = 1.15 \times 10^{-4}$ *and* $\alpha_b = 0.$

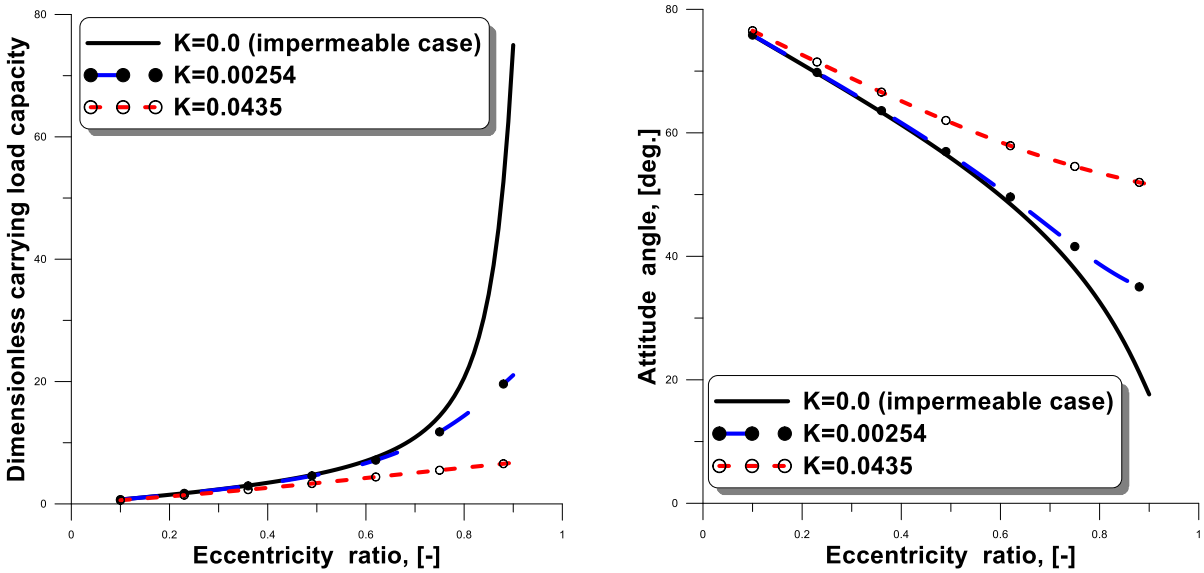

Figure 12. Effects of the permeability K of the porous layer on the hydrodynamic performance of the bearing (carrying load capacity and attitude angle) for $\beta = 0.0$; $\bar{\ell} = 0.1$; $\phi = 10\ \%$; $\bar{\mathcal{L}} = 1.15 \times 10^{-4}$; *and* $\alpha_b = 0.$

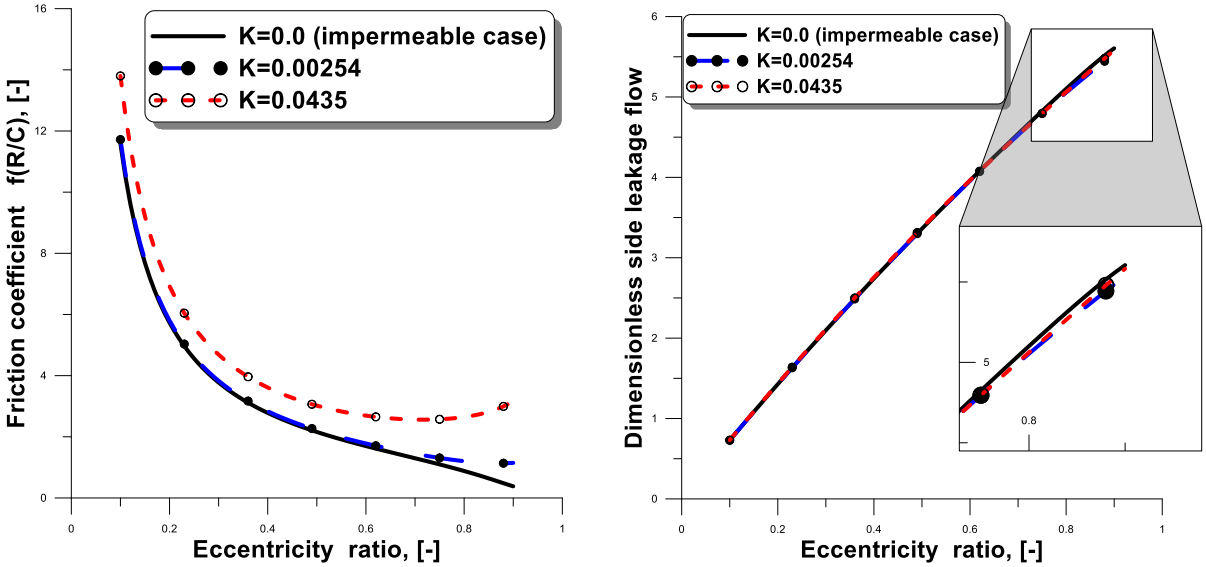

Figure 13. Effects of the layer's permeability $\boldsymbol{K}$ on the hydrodynamic performance of the bearing (friction coefficient and side leakage flow) for $\boldsymbol{\beta = 0.0}$; $\boldsymbol{\bar{\ell} = 0.1}$; $\boldsymbol{\phi = 10\ \%}$; $\boldsymbol{\bar{\mathcal{L}} = 1.15 \times 10^{-4}}$; *and* $\boldsymbol{\alpha_b = 0.}$

Figures 12 and 13 give the effects of the permeability K of the porous matrix on the hydrodynamic performance of the porous journal bearing for eccentricity ratios varying from 0.1 to 0.90. For the same operating eccentricity ε, we observe: an increase in the attitude angle φ and the coefficient of friction $f(R/C)$ with K; a decrease in bearing load capacity with K. On the other hand, the leakage flow rate is not significantly affected by the permeability even for high eccentricities.

Effects of the volume fraction $\boldsymbol{\phi}$ *of the NPs, the elasticity factor* $\boldsymbol{\bar{\mathcal{L}}}$*, the slip coefficient* $\boldsymbol{\alpha_b}$ *and the penetration coefficient* $\boldsymbol{\beta}$ *on the pressure*

Figures 14 to 16 represent the hydrodynamic pressure profiles determined for different values of the volume fraction ϕ, of the elasticity factor $\bar{\mathcal{L}}$, and the Beavers-Joseph slip coefficient α_b.

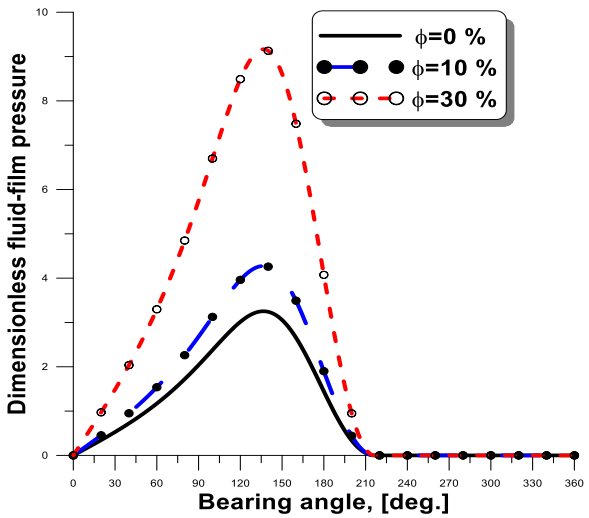

Figure 14. Pressure profiles calculated at $\boldsymbol{\bar{z} = 0}$ for different volume fractions $\boldsymbol{\phi}$, $\boldsymbol{\varepsilon = 0.6}$; $\boldsymbol{\bar{\ell} = 0.1}$; $\boldsymbol{\bar{\mathcal{L}} = 1.15 \times 10^{-4}}$; $\boldsymbol{\alpha_b = 0.}$; $\boldsymbol{K = 4.35 \times 10^{-2}}$; *and* $\boldsymbol{\beta = 0.}$

The influence of these parameters on the pressure can be summarized as follows:

- The pressure in the film increases with the volume fraction of the NPs since the viscosity of the nanolubricant is an increasing function of the concentration according to the Krieger-Dougherty viscosity model as depicted in Figure 14.
- Consideration of the elasticity of the fluid film-porous layer interface leads to a substantial drop in pressure due to an increase in film thickness accompanied by an extension of the active area of the bearing as shown in Figure 15.
- The effect of the slip velocity at the fluid film-porous layer interface on the pressure cannot be neglected, especially for low values of the Beavers-Joseph slip coefficient α_b (Figure 16).

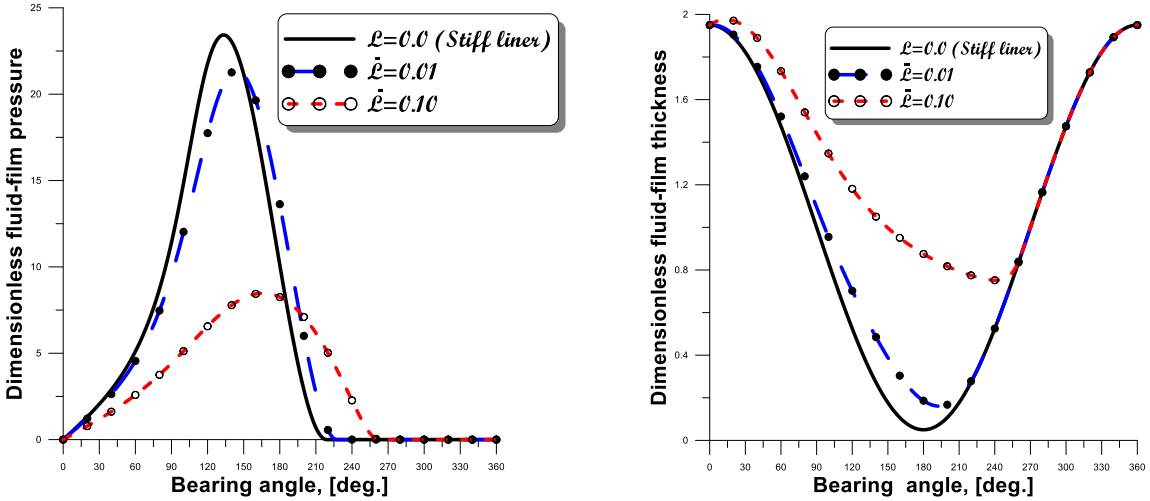

Figure 15. Pressure profiles of and thickness of the film calculated at $\bar{z} = 0$ for different values of the elasticity factor $\bar{\mathcal{L}}$, $\phi = 30\%$; $\varepsilon = 0.95$; $\bar{\ell} = 0.4, \alpha_b = 0.$; $K = 4.35 \times 10^{-2}$; *and* $\beta = 0$.

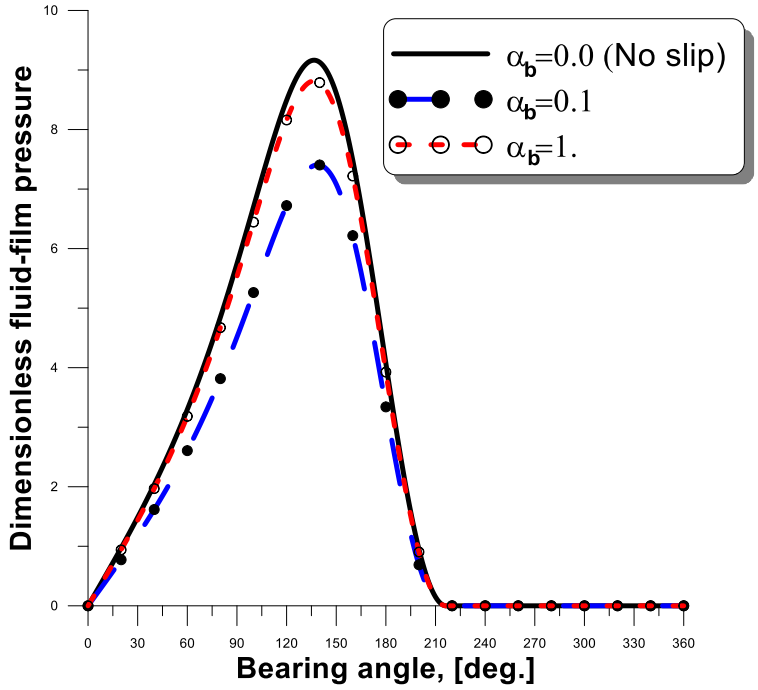

Figure 16. Pressure profiles calculated at $\bar{z} = 0$ for different values of the Beavers-Joseph slip coefficient α_b, $\bar{\mathcal{L}} = 6 \times 10^{-6}$; $\phi = 30\%$; $\varepsilon = 0.60$; $\bar{\ell} = 0.1$; $K = 4.35 \times 10^{-2}$; *and* $\beta = 0$.

Conclusions

The main objective of this research work was to rigorously analyze the elastohydrodynamic behavior of finite length porous journal bearings operating in isothermal regime and involving laminar flows of rheologically complex nanolubricants modeled as non-Newtonian polar fluids with couple-stresses effects. The aim was to set up efficient numerical simulation codes to aid in the design of porous bearings. The choice of this fluid model makes possible to take into consideration the characteristic size of the nanoparticles (NPs) added to the base lubricant. In this paper, we have studied the influence of some key parameters, namely: the characteristic size and the concentration of NPs on the steady-state performance characteristics of a finite length compliant porous plain bearing by solving the direct PEHD lubrication problem; i.e. the case of the bearing operating at an imposed eccentricity ratio ε. The non-Newtonian behavior of the nanolubricant was considered by adopting the V. K. Stokes micro-continuum theory. The modified Reynolds equation, considering the elastic deformation of the porous bearing and the Beavers–Joseph slip conditions at the fluid film–poroelastic bearing interface was derived within the context of thin fluid films lubrication theory.

The permeability of the porous medium was successfully introduced into the modified Reynolds equation using the Morgan-Cameron approximation in the case of a very thin porous layer ($H/R \ll 1$). This further simplified the numerical solution of the direct PEHD problem and thus avoided making the coupling between the modified Reynolds equation and the modified Darcy's equation governing the flow of the polar nanolubricant in the porous medium using an iterative procedure.

The elastic deformation of the fluid film-porous layer interface was predicted by the simplified analytical thin elastic layer model. The modified Reynolds equation was normalized then discretized and solved by the finite difference technique using a nine point calculation stencil (molecule).

The developed model based on the Cameron-Morgan approximation was successfully validated by comparing the theoretical results with the experimental measurements carried out by Mokhtar et al. in the case of a Newtonian lubricant and a porous bearing (89% copper, 10% Tin, 1% Graphite) obtained by sintering (powder technology). A second validation was made by comparing the results obtained by the developed computer code with the theoretical results published by Rouleau et al.(1974).

The parametric study highlighted the non-negligible effects of certain key parameters related to the formulation of modern nanolubricants, namely the characteristic size and the concentration of NPs (fullerenes) or agglomerates of NPs. The results from the various numerical simulations carried out are summarized as follows:

- For an imposed operating eccentricity, the size and concentration of NPs increase the pressure and therefore the load capacity of the journal bearing system, while the attitude angle, the leakage flow rate, and the coefficient of friction decrease. The combined effects of the size and the concentration of the NPs are more significant as the operating eccentricity is high.
- The pressure in the fluid film, the carrying capacity, and the leakage rate decrease with the permeability of the porous layer. However, the attitude angle and the coefficient of friction increase.
- The deformation of the porous layer due to pressure significantly affects the pressure distribution and the geometry of the film, especially for large operating eccentricities and low values of Young's elasticity modulus.
-

The results obtained provide interesting information for the designers of porous bearings as well as the manufacturers of lubricants.

Scientific Ethics Declaration

The authors declare that the scientific ethical and legal responsibility of this article published in EPSTEM journal belongs to the authors.

Acknowledgements or Notes

* This article was presented as a poster presentation at the International Conference on Technology, Engineering and Science (www.icontes.net) held in Antalya/Turkey on November 16-19, 2023.

References

Ariman, T., Turk, M. A., & Sylvester, N. D. (1974). Applications of micro-continuum fluid mechanics. *International Journal of Engineering Science, 12*(4), 273–293.

Bujurke N. M., &Naduvinamani, N. B. (1991). On the performance of narrow porous journal bearing lubricated with couple stress fluid. *Acta mechanica, 86*(1), 179–191.

Beavers, G. S., & Joseph, D. D. (1967). Boundary conditions at a naturally permeable wall. *Journal of Fluid Mechanics, 30*(1), 197–207.

Cosserat, E., & Cosserat, F. (1909). *Théorie des corps déformables.* Librairie

Darcy, H. (1856). *Les fontaines publiques de la ville de Dijon*. In V. Dalmont (Ed.). Paris.

Elsharkawy, A. A., & Guedouar, L. H. (2001). Direct and inverse solutions for elastohydrodynamic lubrication of finite porous journal bearings. *Journal of Tribology, 123*(2), 276–282.

Elsharkawy, A. A., & Guedouar, L. H. (2001). Hydrodynamic lubrication of porous journal bearings using a modified Brinkman-extended Darcy model. *Tribology International, 34*(11), 767–777.

Hamrock, B. J., Schmid, S. R., & Jacobson Bo, O. (2004). *Fundamentals of fluid film lubrication* (2nd ed.). Marcel Dekker, Inc.

Krieger, I. M., & Dougherty, T. J. (1959). A mechanism for nonnewtonian flow in suspensions of rigid spheres. *Transactions of the Society of Rheology, 3*(1), 137-152.

Kaneko, S., Inoue, H., & Ushio, K. (1994). Experimental study on mechanism of Lubrication in Porous Journal Bearings: Oil film formed in bearing clearance. *JSME International Journal. Ser. C, Dynamics, Control, Robotics, Design and Manufacturing, 37*(1), 185–192.

Lahmar, M., (1991).*Modélisation du comportement élastohydrodynamique des revêtements de surface dans les paliers hydrodynamiques.* (Doctoral dissertation).Poitiers University.

Lahmar, M. (2005). Elastohydrodynamic analysis of double-layered journal bearings lubricated with couple stress fluids. *Proceedings of the Institution of Mechanical Engineers, Part J: Journal of Engineering Tribology, 219*(2), 145-165.

Lin, J. R., Hwang, C. C., & Yang, R. F. (1996). Hydrodynamic lubrication of long, flexible, porous journal bearings using the Brinkman model. *Wear, 198*(1), 156–164.

Lin, J. R. & Hwang, C.C. (1993). Lubrication of short porous journal bearings–use of the Brinkman-extended Darcy model. *Wear, 161*(1–2), 93–104.

Lin, J. R., & Hwang, C. C. (1994). Hydrodynamic lubrication of finite porous journal bearings–use of the Brinkman-extended Darcy model. *International Journal of Mechanical Sciences, 36*(7), 631–644.

Mak, W. C., & Conwy, H. D. (1977). The lubrication of a long, porous, flexible journal bearing. *Journal of Lubrication Technology, 99*(4), 449–454.

Morgan, V. T., &Cameron, A. (1957). Mechanism of lubrication in porous metal bearings. In Proceedings of the *Conference on Lubrication and Wear* (Vol. 89,151-157). London

Mokhtar, M. O. A., Rafaat, M., & Shawki, G. S .A (1984). *Experimental investigations into the performance of porous journal bearings (*No.840097). SAE Technical Paper

Naduvinamani, N. B., Hiremath, P. S., & Fathim, S. T. (2002). Lubrication of a narrow porous journal bearing with a couple stress fluid. *Lubrication Science, 14*(4), 393–413.

Prakash, J., & Vij, S. K. (1974). Analysis of narrow porous journal bearing using Beavers-Joseph criterion of velocity slip. *Journal of Applied Mechanics, 41*(2), 348–354.

Naduvinamani, N. B., Hiremath, P. S., & Gurubasavaraj,, G. (2001). Static and dynamic behaviour of squeeze-film lubrication of narrow porous journal bearings with coupled stress fluid. *Proceedings of the Institution of Mechanical Engineers, Part J: Journal of Engineering Tribology, 215*(1), 45–62.

Oliver, D. R. (1988). Load enhancement effects due to polymer thickening in a short model journal bearing. *Journal of Non-Newtonian Fluid Mechanics, 30*(2–3), 185–196.

Rouleau, W. T., & Steiner, L. I. (1974). Hydrodynamic porous journal bearings. part i—finite full bearings. *Journal of Lubrication Technology, 96*(3), 346–353.

Scott, W., &Suntiwattana, P. (1995). Effect of oil additives on the performance of a wet friction clutch material. *Wear, 181*, 850–855.

Stokes, V. K. (1966). Couple stresses in fluids. The Physics of Fluids, *9*(9), 1709–1715.

Stokes, V. K. (1984). *Theories of fluids with microstructures: An introduction*, Springer Science & Business Media.

Trachsel, M., Pittini, R., & Dual, J. (2017). A combined approach to study and model the effect of viscous heating in small porous, self-lubricating journal bearings. *Tribology International, 116,* 199–207.

Author Information

Mustapha Lahmar
University 8th may 1945 Guelma
BP 401, Guelma University, Guelma (24000)
Contact e-mail: *lahmar.mustapha@univ-guelma.dz*

Ammar Athmania
University 8th may 1945 Guelma
BP 401, Guelma University, Guelma (24000)

Benyebka Bou-Said
Université de Lyon, LaMCoS, INSA Lyon
Bâtiment Sophie Germain
27bis, Avenue Jean Capelle
F69621 Villeurbanne cedex
France

To cite this article:

Lahmar, M., Athmania, A., & Bou-Said, B. (2023). Numerical modeling and simulation of a poroelastic journal bearing lubricated by nanofluids with couple-stresses. *The Eurasia Proceedings of Science, Technology, Engineering & Mathematics (EPSTEM), 26,* 604-623.